Accurate visualization and quantification of coronary vasculature by 3–D/4–D fusion from biplane angiography and intravascular ultrasound

Andreas Wahle, Steven C. Mitchell, Mark E. Olszewski, Ryan M. Long, and Milan Sonka

Department of Electrical and Computer Engineering
The University of Iowa, Iowa City, IA 52242–1527, U.S.A.

ABSTRACT

In the rapidly evolving field of intravascular ultrasound (IVUS) for tissue characterization and visualization, the assessment of vessel morphology still lacks a geometrically correct 3-D reconstruction. The IVUS frames are usually stacked up to form a straight vessel, neglecting curvature and the axial twisting of the catheter during the pullback. This paper presents a comprehensive system for geometrically correct reconstruction of IVUS images by fusion with biplane angiography, thus combining the advantages of both modalities. Vessel cross-section and tissue characteristics are obtained from IVUS, while the 3-D locations are derived by geometrical reconstruction from the angiographic projections. ECG-based timing ensures a proper match of the image data with the respective heart phase. The fusion is performed for each heart phase individually, thus yielding the 4-D data as a set of 3-D reconstructions.

Keywords: Image and Data Fusion, 3-D/4-D Reconstruction, Segmentation, Intravascular Ultrasound, Biplane Angiography, Cardiovascular System, Tissue Characterization, Visualization, Volumetry.

1. INTRODUCTION

Heart attack and stroke are the major causes of human death; almost twice as many people die from cardiovascular diseases than from all forms of cancer combined. A number of imaging modalities exists to help diagnose coronary artery disease. Among them, X-ray coronary angiography and intravascular ultrasound (IVUS) represent the most commonly used diagnostic tools. Selective coronary angiography provides projectional X-ray images of contrast-filled coronary vessels and has been clinically used for decades. Several semi-automated tools are available for evaluation of local obstructions *(stenoses)*.[1–4] A substantial drawback of angiography is that, while it provides detailed images of the vessel lumen, it offers no information about the extent and the composition of the plaque covering the inner coronary wall. The lumen outline allows an indirect assessment of the plaque only, especially in the case of diffuse coronary artery diseases, where no local obstructions are given.[4–6]

Intravascular ultrasound of the coronary arteries is becoming a well-established complementary method to angiography for cardiovascular diagnosis and supervision of coronary interventions. The vessel cross-sections can be imaged by inserting an ultrasonic transducer directly into the vessel lumen, mostly through the femoral artery. In this way, the lumen as well as the vessel wall are depicted accurately, including information about the composition and location of the plaque.[4,7–10] This information is essential for both planning interventions (e.g. for stenting or angioplasty) and for monitoring their success. A major drawback of IVUS is its inability to consider the vessel curvature and the orientation of the imaging catheter when assigning the detected plaque to specific locations. Conventional 3-D methods simply stack the IVUS frames as acquired during a constant-speed pullback of the catheter, thus covering a specific segment of usually a few centimeters. While this method works well in straight vessels,[11] it introduces substantial errors in volumetric estimations when applied to tortuous vessel segments.[12,13]

The image data acquired from biplane angiography, and usually needed for catheter guidance during the IVUS intervention, can be utilized to accurately reconstruct the path and orientation of the IVUS catheter in 3-D and 4-D (i.e. 3-D plus time, where *time* specifies any phase of the heart cycle). During this fusion process, the relative and absolute orientations of the IVUS frames are determined using our previously reported system for establishing the absolute orientation in 3-D on still images.[14–16] Finally, the reconstructed result can be either utilized for visualization or for geometrically correct quantifications. The entire process can be split up into the following list of tasks:

E-mail: <andreas-wahle@uiowa.edu>, http://www.engineering.uiowa.edu/~awahle; Fax: +1-319-335-6028

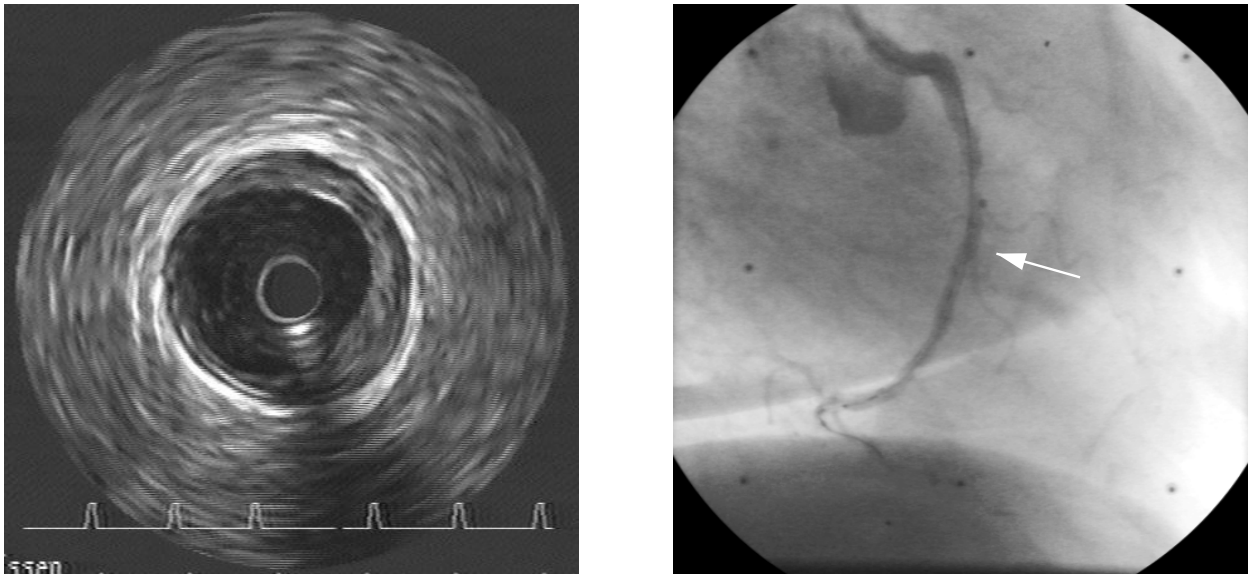

Figure 1. Images from intravascular ultrasound (left, with ECG signal inserted) and angiography (right) of the same vessel (in-vivo right coronary artery, arrow in the angiogram indicates approximate location of the IVUS frame); note that the IVUS catheter is slightly visible in the angiogram.

1. Acquire IVUS and angiographic data and sort them by the heart phase;
2. segment IVUS and angiographic data for vessel and tissue structure;
3. determine the 3-D location for each feature in each considered heart phase;
4. use the reconstructed 3-D or 4-D data for visualization and/or quantification.

The Methods section is structured according to this list.

2. METHODS

2.1. Data Acquisition

IVUS and angiographic data are acquired independently from each other. For the 4-D case in-vivo, separate sets of IVUS frames and corresponding angiographic images are acquired for each heart phase according to the ECG signal. An example is shown in Figure 1.

2.1.1. Intravascular ultrasound

Currently, there are two major kinds of IVUS devices available, mechanically driven catheters and solid-state devices.[10] Mechanically driven catheters consist of a flexible sheath, a core which contains the transducer in its tip, and an external motor which rotates the core. Solid-state devices generate images from a transducer array and contain no moving parts. The data is usually stored on S–VHS tapes and has to be digitized afterwards.[15–17] The transducers commonly used have a fixed frequency of 20–30 MHz; frequencies of 40–45 MHz recently became available as well. The size of the catheter (diameter) is between 2.9F and 3.2F, where 1F (one *French*) corresponds to $\frac{1}{3}$mm.

Obviously, the IVUS catheter delivers an image which represents the vessel cross section at the current location only. Motorized continuous pullback ensures that a specific vessel segment is covered, and that the location can be approximated from the time passed since the pullback started. The sheathed design of mechanically driven catheters has the major advantage of providing a stable pullback path, since only the core is moving in the direction of the pullback and the sheath remains in its position. This is currently a requirement of our fusion method, since the catheter path is predicted from a single angiographic pair taken at the start of the pullback.[15–17] In order to find the correct set of IVUS frames corresponding to the same heart phase, it furthermore has to be ensured that the ECG data are recorded synchronously. Merging of images from different heart phases introduces unacceptable errors.[10,18]

2.1.2. Biplane angiography

The biplane angiograms are taken immediately at the start of the pullback and cover at least one heart cycle. They are used to extract the catheter path automatically along the expected pullback trajectory, and to find the vessel outline as a reference for the following fusion process. Angiographic data is usually stored on 35 mm cine film, video tape, or on digital media.[19] Recordable Compact Discs (CD–R) in DICOM format are becoming the new standard in cath-labs,[4] and can be read with appropriate viewers. For DICOM media, we have developed a browser based on the PAPYRUS-toolkit.[20] The digital format has the major advantage that the parameters of the selected imaging geometry, used as basis for the angiographic 3-D reconstruction,[6,21] are available along with their corresponding image data.

As shown before,[4] angiographic imaging is subject to substantial distortions, thus the images have to be rectified *(dewarped)* for the so-called pincushion distortion and sigmoidal effects. While this distortion can often be neglected in semi-automated single-plane analysis of local stenosis,[22] 3-D reconstruction techniques require a more careful correction of these effects.[23] For the purpose of the fusion approach, an eight-point dewarping[24] has shown the best ratio of organizational and computational effort in relation to the accuracy.

2.2. Segmentation

2.2.1. Basic border detection methods for IVUS

A comprehensive overview about the different approaches for detecting the inner and outer borders of the vessel wall was presented previously.[10] They include simulated annealing, active contour and active surface methods *(snakes)*, as well as graph-search and dynamic programming.[25] While our initial segmentation method basically worked on each IVUS frame separately and adjusted the region-of-interest (ROI) from frame to frame,[8,9] we meanwhile adopted the approach to perform a segmentation in longitudinal direction through the IVUS stack to derive the local ROI's.[11,26] An in-vitro example showing the entire segmentation process is presented in Figure 2.

2.2.2. Knowledge-based IVUS segmentation

Most IVUS segmentation methods are based on local gray-level changes (borders) only, despite the fact that many features produce unique patterns in ultrasound images by which they can be identified. Therefore, it seems to be advantageous for the segmentation process to utilize this nature and to look for specific patterns in the ultrasonic echo. Our knowledge-based segmentation method as described in detail elsewhere[8] automatically identifies the plaque/media interface (internal lamina, internal wall border), the media/adventitia interface (external lamina, external wall border), and the plaque/lumen interface (plaque border). Due to the use of a-priori information about the 2-D and 3-D anatomy of coronary vessels and ultrasound imaging physics, the method can automatically determine vessel wall morphology and plaque areas. The two key aspects of the approach are as follows:

1. Graph searching[25] is utilized to identify globally optimal borders;
2. a-priori information is incorporated into the detection process through the computation of local cost values.

In particular, to identify the position of the internal and external wall borders, the method searches for edge triplets representing the leading and trailing edges of the laminae echoes. The given ROI serves as a model of the preferred vessel shape. Knowledge of the vessel wall thickness is also used to constrain the search for the external and internal wall borders.

2.2.3. Texture-based tissue characterization

In the presence of plaque, it is frequently desired to obtain further information about the *composition* of the plaque. Roughly, two kinds of plaque can be distinguished by their ultrasonic echoes:[9]

- Hard plaques are composed of fibrous tissue, often in complex layers. In IVUS images, hard plaques are highly reflective of ultrasound and produce bright echoes similar to the adventitia (Fig. 3). Calcified hard plaque regions are typically identified by high-amplitude echo signals with complete distal *shadowing*.
- Soft plaques usually consist of highly cellular areas of intimal hyperplasia and often contain cholesterol, thrombus, and loose connective tissue types. Ultrasound images of soft plaque are characterized by weaker and more texturally homogeneous echoes with lower contrast.

IVUS–Segmentation:

1. Select $n \geq 2$ slicing planes for the longitudinal resampling;
2. perform segmentation for lumen and wall borders in longitudinal images;
3. define cross sectional preliminary borders by connecting guide points from longitudinal segmentation with splines;
4. define cross sectional ROI's within a specifiable distance from those splines;
5. within the cross sectional ROI's, perform segmentation for lumen and wall borders in each IVUS frame.

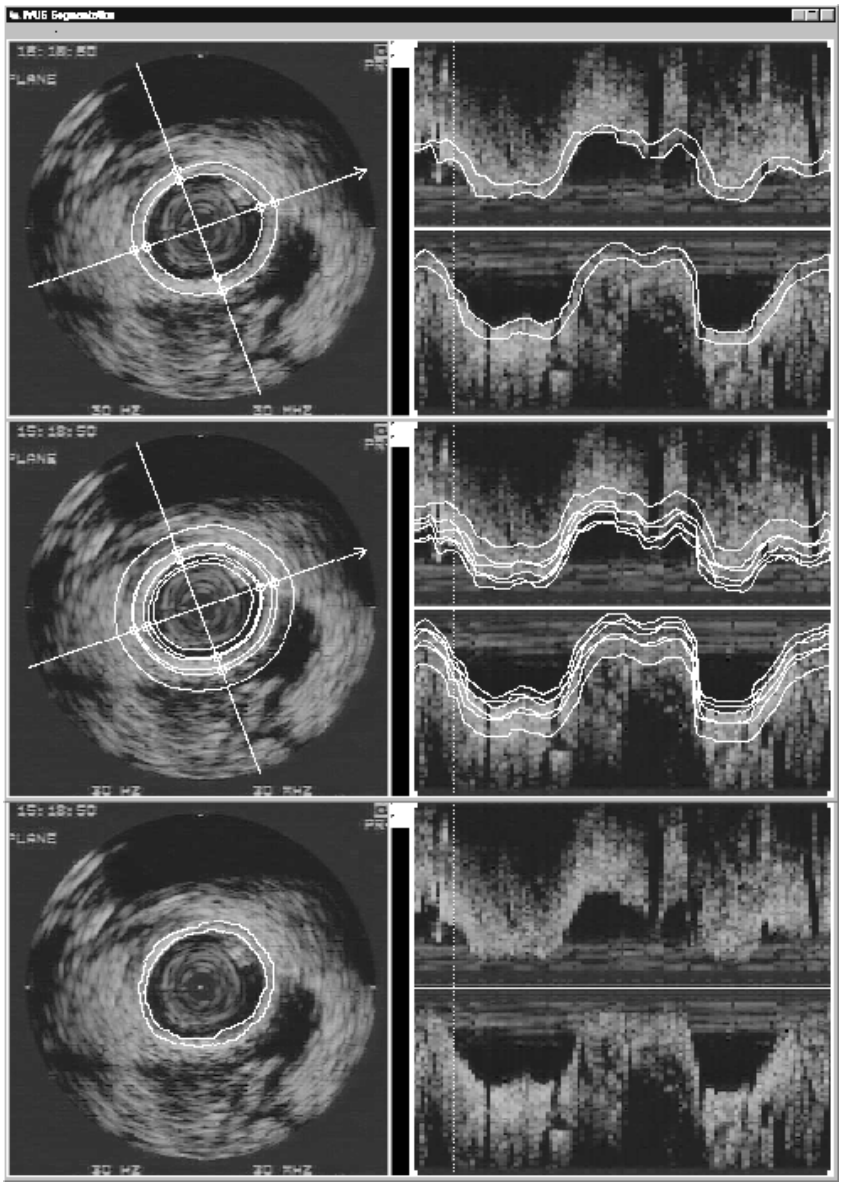

Figure 2. Process of IVUS segmentation using dynamic programming (left window: IVUS frame, right: straight longitudinal view); the user can perform corrections at any time during the segmentation.

To assess plaque composition, plaque type is determined in narrow plaque wedges called *elementary regions*. Classification labels are assigned to the pixel-of-interest P associated with each elementary region. Prior to defining the elementary regions, the entire plaque region A is straightened into a rectangular region B of a constant height H along the plaque/lumen interface (Fig. 4a). The width W of the straightened region B is equal to the length of the plaque/lumen border. In each of the elementary regions, four texture descriptors (gray-level based, co-occurence, run-length, and fractal properties)[9] are evaluated. Plaque wedges may contain a mixture of soft and hard plaque. Consequently, for each wedge containing hard plaque, the plaque wedge may appear as a two- or three-layered structure along the y direction: hard plaque/shadow, or soft plaque/hard plaque/shadow.

After determining for each pixel if it represents plaque, and its classification into either hard or soft plaque according to the set of texture descriptors, the result can be transformed back into the IVUS frames and used for color-coding within the visualization step (Fig. 4b).

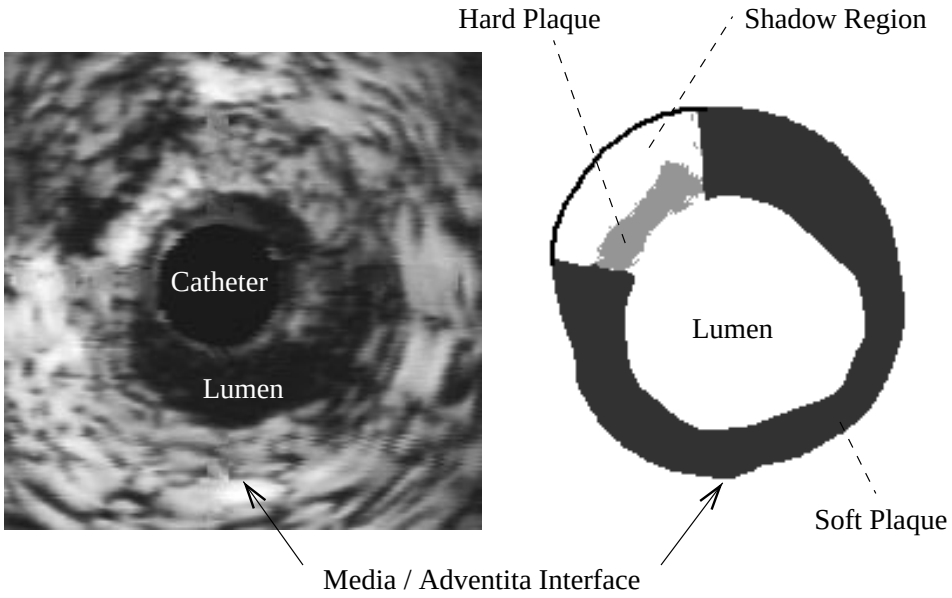

Figure 3. IVUS image of a vessel cross section with a large amount of soft plaque and a radial section of hard plaque in the upper right region; on the right, the computerized classification results are shown.

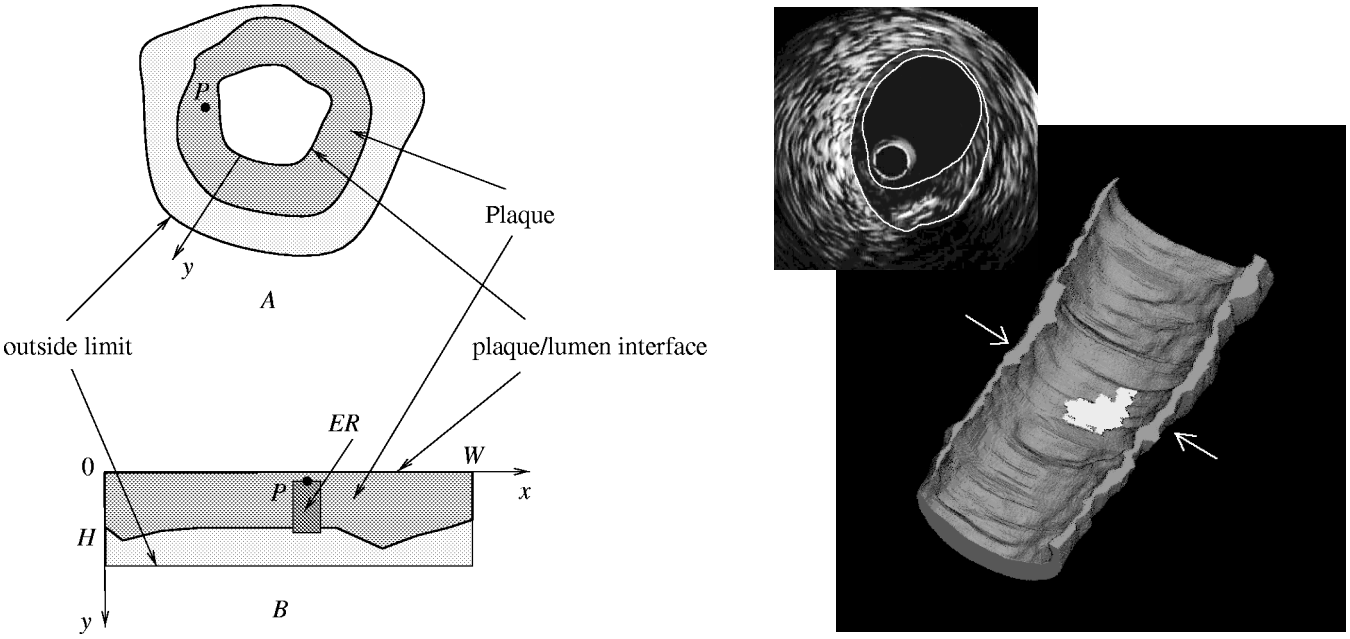

Figure 4. (a) Plaque region straightened along the plaque border: Original plaque region A, straightened plaque region B, example for a point-of-interest P and its associated elementary region ER; (b) straight IVUS reconstruction of a vessel cross section with asymmetric plaque distribution and a region of hard plaque, shown here in white; arrows indicate the location of the depicted IVUS frame.

2.2.4. Catheter trajectory and vessel outline from biplane angiography

The fusion process requires information about the 3-D pullback path, considering the catheter deformation for each heart phase in 4-D. Furthermore, the vessel outline is needed as a reference to determine the absolute orientation of the IVUS data in 3-D space. Given the two time-equivalent 2-D projections of the catheter and the vessel lumen, they can be reconstructed into 3-D based upon the known X-ray gantry positions and orientations during the acquisition process.[6] Several vessel detection algorithms are known from single-plane quantitative coronary angiography (QCA).[1–4] They are usually based on dynamic programming, with the cost matrices created from the first and second derivatives of the gray values perpendicular to the vessel orientation *(profile)*. This initial result can be refined locally by specialized algorithms.[3,4]

While these methods provide excellent results for the purpose of QCA, the catheter detection required a modification of the cost functions. To detect the vessel outline, the extracted catheter is used as limit for the left and right borders. As shown in Figure 5, the user has to mark the start and end points of the pullback only, along with some intermediate points, which are then connected using Catmull–Rom splines.[27] This yields already a good estimate for the catheter path. Within the marked region of interest, first the catheter is extracted (local peak along the vessel profile), then the vessel outline. This data is afterwards reconstructed into 3-D,[6,15] thus providing the necessary geometrical information for the determination of the 3-D catheter pullback trajectory.

The high accuracy of the imaging geometry as required for 3-D volumetric measurements from *only* biplane angiography[6] is not necessary for the purpose of the angiography–IVUS fusion. If the vessel volume is determined from the angiographically reconstructed contours, a linear error in calibration results in a third-power error for the volume. In contrast, errors from calibration remain linear for the reconstruction of the 3-D catheter path and are usually neglectable for the determination of the IVUS frame orientation. Therefore, the angiographic imaging geometry is primarily determined from the known gantry parameters. In addition, the user has to mark a single reference point (Fig. 5) to consider any gravitational effects on the gantry.

2.3. IVUS/Angiography Fusion

The reconstruction and fusion of the data provided by both modalities is a complex registration problem and has been approached by several other groups as well.[28–31] In general, the movement pattern of the catheter during the pullback has to be determined as accurately as possible, and afterwards the set of 2-D IVUS data mapped into 3-D space. Thus, the problem of assigning the IVUS data into 3-D space is two-fold:

1. The IVUS frames have to be related to 3-D locations, and
2. their orientations have to be determined.

When sheathed catheters are used, the location of any IVUS frame with known acquisition time can be determined by figuring the time passed from the start of the pullback until this specific frame was taken. Using the reconstructed catheter path, the segment previously visited by the transducer can be easily measured, and thus the location reached after imaging this previous vessel segment can be established. The more complicated task is the identification of the spatial orientation of a frame, which has been discussed in detail previously.[14–17] The *relative* changes in orientation between adjacent IVUS frames can be determined analytically based upon the Frenet–Serret formulas.[32] However, the *absolute* orientation in 3-D remains ambiguous. The problem is comparable to fitting a sock on a leg:[28] While the leg (catheter path) is stable, the sock (axial frame orientation) can freely be rotated around the leg, but fits optimally only in one orientation.

To solve this problem, we have developed a non-iterative statistical approach, which calculates the optimum match of the frame set directly in 3-D from an arbitrary initial orientation.[14–16] From the 3-D catheter path as extracted before, the relative catheter twist is estimated based upon a discrete version of the Frenet–Serret formulas, the *sequential triangulation method*.[17] The vessel lumen has already been segmented in both IVUS image data and angiograms, where the angiographic lumen is represented in 3-D by elliptical contours derived from the 2-D outlines. In both data sets, the *out-of-center position* of the imaging catheter relative to the lumen is determined. Then, the IVUS data is mapped into 3-D using the initial orientation along with the relative twist. For each frame location, the *out-of-center strength* and the *difference angles* of angiographic vs. IVUS reconstructions are determined. Within a moving window of arbitrary but fixed size, a statistical analysis is performed. A *reliability weight* is calculated for each location of the moving window, giving higher weight to locations with high out-of-center strength, and limiting

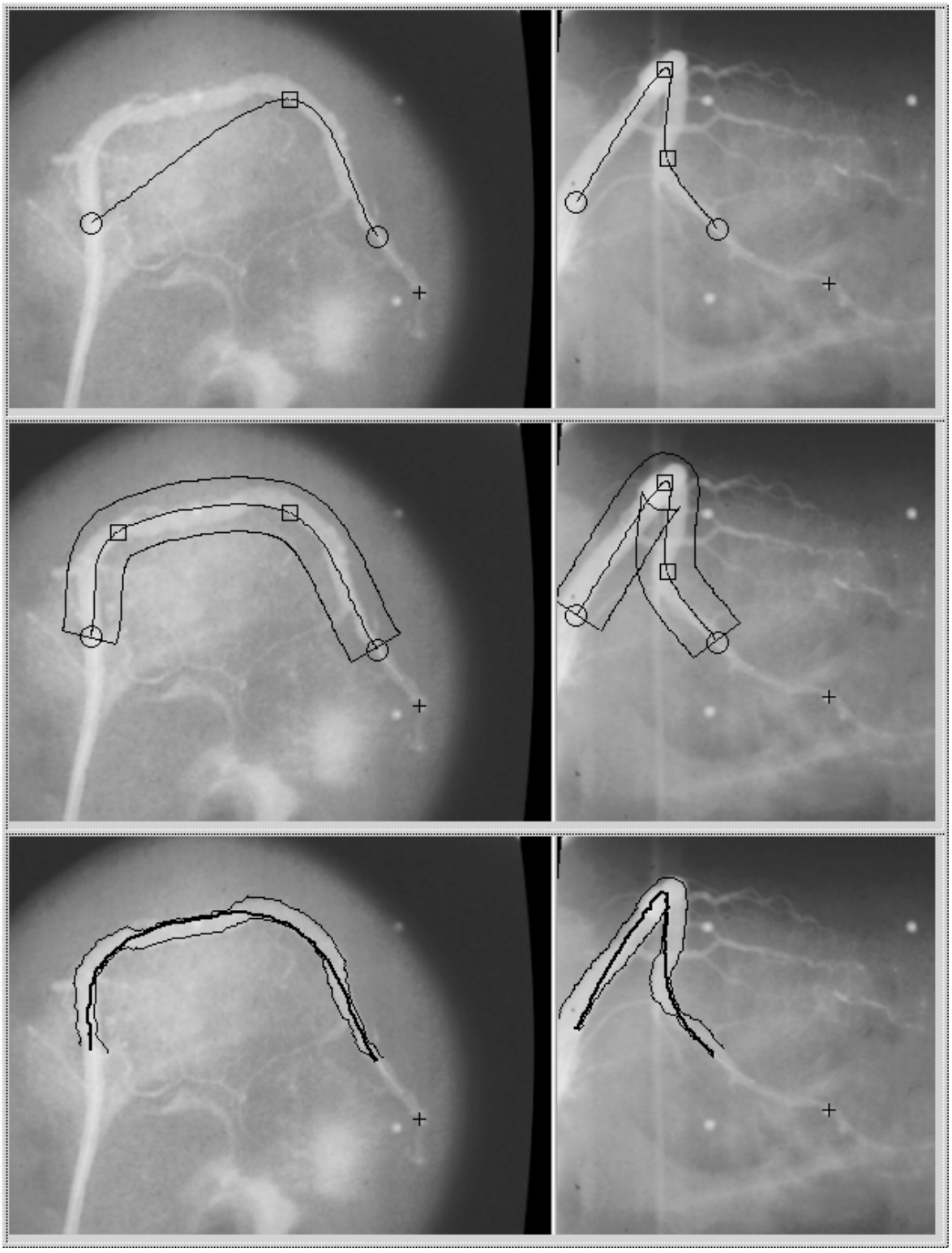

Figure 5. Extraction of the catheter path and outline of the vessel lumen from both angiograms within interactively defined regions of interest; the cross marks the reference point for automatic adjustments of the imaging geometry.

those with a high standard deviation of the difference angle function, which indicates local distortions. A single correction angle is determined and applied to all IVUS frames relative to the initial orientation.

After mapping the IVUS data and all related contour information into their respective 3-D locations within the geometrically correct oriented frames, the 3-D data set for the specific heart phase is finalized. In the 4-D case, this process is repeated for all selected heart phases separately, i.e. there is currently no usage of information that may be utilized from adjacent phases.

2.4. Evaluation

2.4.1. Visualization of the 3-D/4-D data

As a first step, the resulting 3-D model(s) can be visualized. This is based on automated encoding of the derived contour data in VRML (Fig. 6). For each heart phase, one 3-D indexed face set is created per contour. To obtain a 4-D visualization, VRML time sensors are utilized. If the catheter path or the vessel centerline only are to be visualized, they can be modeled as a set of VRML spheres, each of which represents a single frame location and is associated with its own position interpolator. This ensures a smooth and interpolated display of the movement.[33] Common VRML browsers can be used to view and manipulate the scene. If quantitative data has been derived from the contours, these values can be included into the VRML model by color per vertex encoding, thus allowing an easy and fast visual assessment of the lesion or the results of the intervention by the physician.

Another way to display the 3-D data is by using the raw IVUS data to form a cube of *voxels*, as known from tomographic modalities like CT and MR. Therefore, a voxel space of specifiable size is created, and each pixel or contour data of an IVUS frame mapped to a specific voxel. This voxel cube can then be visualized with commonly used tools. However, those are sometimes not sufficient, as the example of the maximum intensity projection (MIP) shows (Fig. 7). For the purpose of geometrically correct IVUS volume visualization, a special projection technique was developed that considers the properties of the IVUS data better than the conventional MIP, the *energy-complement projection* (ECP).[34] In Figure 7, note that the catheter is easily visible and its bending is depicted correctly.

2.4.2. Volumetric quantifications from the reconstructed contours

Quantitative measurements such as wall and plaque thickness can be derived from the contour data as well, actually considering the vessel curvature in contrast to conventional IVUS reconstruction systems. The space between adjacent contours is interpolated to form a volume element. Integrating over an entire vessel segment or any part thereof yields the total volume enclosed by the lumen and/or wall borders. Their difference equals the wall thickness at the respective locations. In angiographic reconstructions, the 3-D contours are restricted to elliptical shapes;[6] the fusion with IVUS data however results in a much more complex model for volumetric quantification, thus requiring new methods.

The well-established method of using generalized conic sections to fill up the space between adjacent contours has been extended by introducing free-shaped base areas.[6,35] In both the elliptic and free-shaped models, local volumes between two adjacent contours are compensated until a geometrically trivial object is reached. Especially, in comparison to methods for CT and MR with parallel slices, it has to be considered that the two base areas may be tilted against each other. While the elliptical case[6] always yields a good approximation since the basic shape (cone) is known a-priori, in the free-shaped version assumptions about the shape of the volume cannot be made. Thus, a compromise had to be reached, which linearly interpolates the areas between the two adjacent contours.[35]

3. RESULTS

The validations of the underlying methods for IVUS segmentation,[8] tissue characterization,[9] and geometrical 3-D reconstruction from biplane angiograms[6] have been described in detail before. The validation of the entire system is ongoing in parallel to the further improvement and integration of its components. So far, the fusion system was extensively tested in computer simulations and phantom studies, and applied in-vivo on routine patient data. Parts of the in-vivo data were acquired at the University Hospital Essen, Germany; at the Brigham and Women's Hospital at Harvard Medical School, Boston MA, U.S.A.; and at the University Hospital Berne, Switzerland. Preliminary results on six patients showed a good performance of the components of our system. Both IVUS and angiographic segmentation algorithms have a high reliability, the 3-D reconstruction and fusion methods were successfully applied in all cases. In addition, VRML visualization could be performed in real-time.

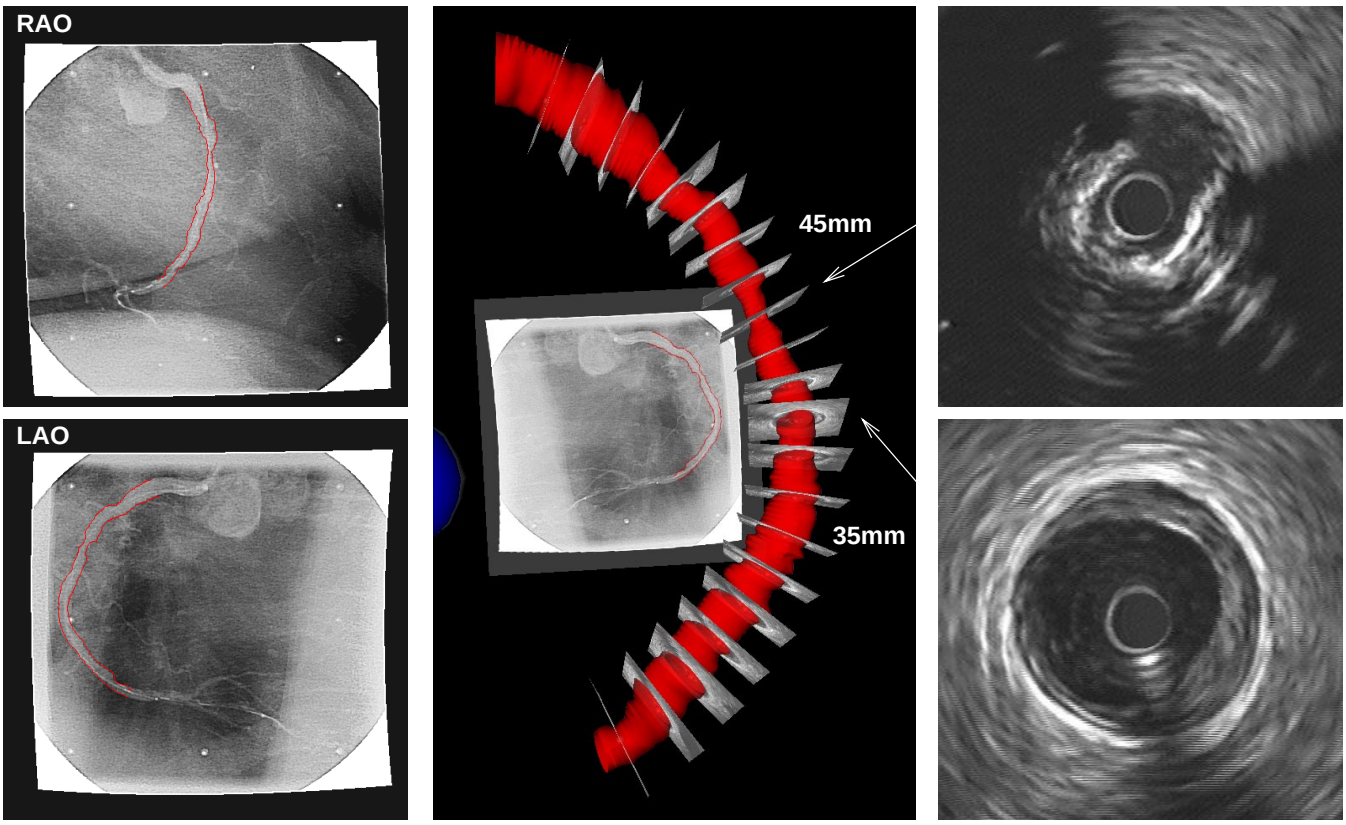

Figure 6. Reconstruction of an in-vivo stenosed right coronary artery and visualization in VRML: Angiograms are shown on the left, selected IVUS frames with soft plaque (35 mm after pullback start) and a strong stenosis with hard plaque (around 45 mm) on the right hand side; center shows the VRML scene with angiograms and selected IVUS frames included in their geometrically correct location, as well as the contours of the segmented lumen.

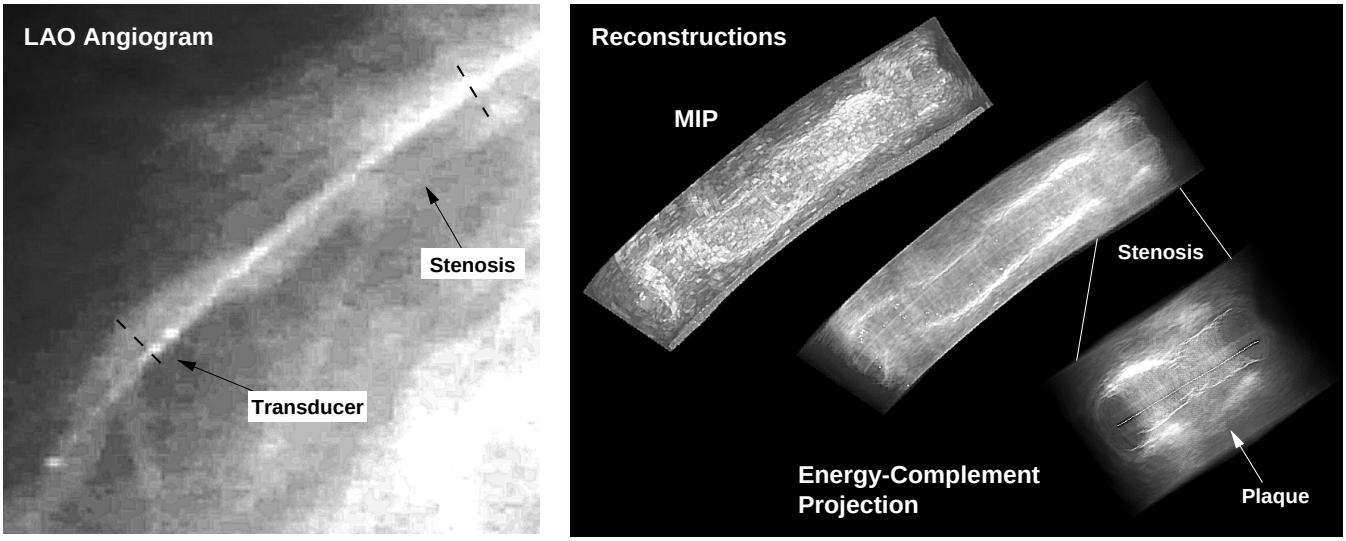

Figure 7. Reconstruction of an in-vivo stenosed left anterior descending artery and visualization by projection techniques: While the conventional maximum intensity projection does not provide acceptable results, the energy-complement projection clearly visualizes the stenotic part, especially after inclusion of the segmented lumen.

While the improvement and validation of the angiographic and IVUS segmentation algorithms are ongoing, the accuracy of the absolute frame orientation as a result of the fusion has been determined. Our in-vitro studies revealed that the sheathed design of the IVUS catheters used provide a stable pullback, but may introduce mapping errors (rms $21.96 \pm 4.87°$) in the axial IVUS frame orientation due to friction effects.[15] In-vivo, the mismatch of the vessel centerline was 0.73 ± 0.35 mm for the most tortuous vessel.[16] The volume quantification method was validated by evaluation of 20 computer-generated 3-D objects using different sampling rates. Test volumes included a mixture of cylindrical, conical, and elliptical shapes, similar to those usually found in undiseased or moderately diseased vessels. Error rates were computed by comparing known volumes of mathematical phantoms to corresponding volumes calculated using the described method from cross-sectional data. All results were obtained using 4–10 frames per volume. For a cylindrical volume with x- and y-dimensional tilting rotations between 5° and 25°, errors ranged from 0.8% to 6.75%, respectively; for a simulated 90% stenosis located in an arc, the error was 4.5% for 10 frames with inclination angles of 1.6° between adjacent contours.[35]

4. DISCUSSION AND CONCLUSIONS

The presented fusion approach provides an accurate assessment of coronary vessels for preparation and validation of interventions and stenting. Results are available with only a few steps of manual interaction in almost real-time. Our methods previously established on still images were successfully extended into 4-D (3-D plus time), thus providing an important aid for coronary interventions.[14–17,33,35] While the underlying segmentation and reconstruction systems were initially developed as stand-alone applications,[6,8,9,17] major efforts are currently in place to integrate all components into a comprehensive system suitable for clinical application. Conventional PC hardware is utilized to keep the system easily transportable and to allow its use by physicians. During this process, the methods are constantly re-evaluated and improved. Some inherent problems, such as the distortions introduced by friction on the mechanically driven IVUS catheter,[15] are to be addressed in the future as well.

The comprehensive fusion system, once finalized, will provide a powerful tool for the analysis of IVUS data. While certain restrictions have to be recognized (automated pullback, ECG-triggering or -gating, biplane angiography, preferably digital access to the data), it allows nearly complete access to the full range of information delivered by both X-ray angiography and IVUS. It can be expected that future improvement of the IVUS technology will further increase the clinical value of a geometrically correct 3-D reconstruction, visualization, and quantitative evaluation of the IVUS data.

ACKNOWLEDGMENTS

This work has been supported in part by grant Wa 1280/1-1 of the *Deutsche Forschungsgemeinschaft* (DFG), Bonn, Germany; and by grant 1 R01 HL63373-01 of the *National Institutes of Health* (NIH), Bethesda MD, U.S.A. Previous support was provided by grant Pr 507/1-2 of the DFG; and by grants IA-94-GS-65 and IA-96-GS-42 of the *American Heart Association* (AHA), Iowa Affiliate. Parts of the in-vivo data presented in this paper were acquired within the scope of an ongoing collaboration with Drs. Clemens von Birgelen and Raimund Erbel, both with the Department of Cardiology at the University Hospital of Essen, Germany.

REFERENCES

1. R. L. Kirkeeide, P. Fung, R. W. Smalling, and K. L. Gould, "Automated evaluation of vessel diameter from arteriograms," in *Proc. Computers in Cardiology 1982, Seattle WA*, pp. 215–218, IEEE-CS Press, (Los Alamitos CA), 1982.
2. J. Beier, H. Oswald, H. U. Sauer, and E. Fleck, "Accuracy of measurement in quantitative coronary angiography (QCA)," in *Computer Assisted Radiology (CAR '91)*, H. U. Lemke, M. L. Rhodes, C. C. Jaffe, and R. Felix, eds., pp. 721–726, Springer, (Berlin/New York), 1991.
3. P. M. J. van der Zwet and J. H. C. Reiber, "A new approach for the quantification of complex lesion morphology: The gradient field transform; basic principles and validation results," *Journal of the American College of Cardiology* **24**, pp. 216–224, July 1994.
4. J. H. C. Reiber, G. Koning, J. Dijkstra, A. Wahle, B. Goedhart, F. H. Sheehan, and M. Sonka, "Angiography and intravascular ultrasound," in *Handbook of Medical Imaging — Volume 2: Medical Image Processing and Analysis*, M. Sonka and M. J. Fitzpatrick, eds., SPIE Press, (Bellingham WA), 2000.

5. C. Seiler, R. L. Kirkeeide, and K. L. Gould, "Basic structure-function relations of the epicardial coronary vascular tree; basis of quantitative coronary arteriography for diffuse coronary artery disease," *Circulation* **85**, pp. 1987–2003, June 1992.
6. A. Wahle, E. Wellnhofer, I. Mugaragu, H. U. Sauer, H. Oswald, and E. Fleck, "Assessment of diffuse coronary artery disease by quantitative analysis of coronary morphology based upon 3-D reconstruction from biplane angiograms," *IEEE Transactions on Medical Imaging* **14**, pp. 230–241, June 1995.
7. Q. Rasheed, P. J. Dhawale, J. Anderson, and J. M. Hodgson, "Intracoronary ultrasound-defined plaque composition: Computer-aided plaque characterization and correlation with histologic samples obtained during directional coronary atherectomy.," *American Heart Journal* **129**, pp. 631–637, Apr. 1995.
8. M. Sonka, X. Zhang, M. Siebes, M. S. Bissing, S. C. DeJong, S. M. Collins, and C. R. McKay, "Segmentation of intravascular ultrasound images: A knowledge-based approach," *IEEE Transactions on Medical Imaging* **14**, pp. 719–732, Dec. 1995.
9. X. Zhang, C. R. McKay, and M. Sonka, "Tissue characterization in intravascular ultrasound images," *IEEE Transactions on Medical Imaging* **17**, pp. 889–899, Dec. 1998.
10. J. Dijkstra, A. Wahle, G. Koning, J. H. C. Reiber, and M. Sonka, "Quantitative coronary ultrasound: State of the art," in *What's New in Cardiovascular Imaging?*, J. H. C. Reiber and E. E. van der Wall, eds., vol. 204 of *Developments in Cardiovascular Medicine*, pp. 79–94, Kluwer, (Dordrecht), 1998.
11. C. von Birgelen, E. A. de Vrey, G. S. Mintz, A. Nicosia, N. Bruining, W. Li, C. J. Slager, J. R. T. C. Roelandt, P. W. Serruys, and P. J. de Feyter, "ECG-gated three-dimensional intravascular ultrasound: Feasibility and reproducibility of the automated analysis of coronary lumen and atherosclerotic plaque dimensions in humans," *Circulation* **96**, pp. 2944–2952, Nov. 1997.
12. J. R. T. C. Roelandt, C. Di Mario, N. G. Pandian, W. Li, D. Keane, C. J. Slager, P. W. de Feyter, and P. W. Serruys, "Three-dimensional reconstruction of intracoronary ultrasound images; rationale, approaches, problems, and directions," *Circulation* **90**, pp. 1044–1055, Aug. 1994.
13. E. Maurincomme and G. Finet, "What are the advantages and limitations of three-dimensional intracoronary ultrasound imaging?," in *Cardiovascular Imaging*, J. H. C. Reiber and E. E. van der Wall, eds., vol. 186 of *Developments in Cardiovascular Medicine*, pp. 243–255, Kluwer, (Dordrecht), 1996.
14. A. Wahle, G. P. M. Prause, C. von Birgelen, R. Erbel, and M. Sonka, "Automated calculation of the axial orientation of intravascular ultrasound images by fusion with biplane angiography," in *Medical Imaging 1999: Image Processing*, K. M. Hanson, ed., vol. 3661, pp. 1094–1104, SPIE Proceedings, (Bellingham WA), 1999.
15. A. Wahle, G. P. M. Prause, S. C. DeJong, and M. Sonka, "Geometrically correct 3-D reconstruction of intravascular ultrasound images by fusion with biplane angiography — methods and validation," *IEEE Transactions on Medical Imaging* **18**, pp. 686–699, Aug. 1999.
16. A. Wahle, G. P. M. Prause, C. von Birgelen, R. Erbel, and M. Sonka, "Fusion of angiography and intravascular ultrasound in-vivo: Establishing the absolute 3-D frame orientation," *IEEE Transactions on Biomedical Engineering — Biomedical Data Fusion* **46**, pp. 1176–1180, Oct. 1999.
17. G. P. M. Prause, S. C. DeJong, C. R. McKay, and M. Sonka, "Towards a geometrically correct 3-D reconstruction of tortuous coronary arteries based on biplane angiography and intravascular ultrasound," *International Journal of Cardiac Imaging* **13**, pp. 451–462, Dec. 1997.
18. N. Bruining, C. von Birgelen, P. J. de Feyter, J. Ligthart, W. Li, P. W. Serruys, and J. R. T. C. Roelandt, "ECG-gated versus nongated three-dimensional intracoronary ultrasound analysis; implications for volumetric measurements," *Catheterization and Cardiovascular Diagnosis* **43**, pp. 254–260, Mar. 1998.
19. J. Beier, U. Krauß, H. Oswald, and E. Fleck, "Archives for coronary angiography: A comparison of cinefilm vs. video vs. digital," in *Proc. Computers in Cardiology 1992, Durham NC*, pp. 263–266, IEEE-CS Press, (Los Alamitos CA), 1992.
20. O. Ratib, H. Hoehn, C. Girard, and C. Parisot, "PAPYRUS 3.0: DICOM-compatible file format," *Medical Informatics* **19**, pp. 171–178, Apr.-June 1994.
21. S. Y. J. Chen and C. E. Metz, "Improved determination of biplane imaging geometry from two projection images and its application to three-dimensional reconstruction of coronary arterial trees," *Medical Physics* **24**, pp. 633–654, May 1997.
22. P. M. J. van der Zwet, D. J. H. Meyer, and J. H. C. Reiber, "Automated and accurate assessment of the distribution, magnitude, and direction of pincushion distortion in angiographic images," *Investigative Radiology* **30**, pp. 204–213, Apr. 1995.

23. A. Wahle, U. Krauß, H. Oswald, and E. Fleck, "Inter- and extrapolation of correction coefficients in dynamic image rectification," in *Proc. Computers in Cardiology 1997, Lund SE*, vol. 24, pp. 521–524, IEEE Press, (Piscataway NJ), 1997.
24. G. P. M. Prause, S. C. DeJong, C. R. McKay, and M. Sonka, "Semi-automated segmentation and 3-D reconstruction of coronary trees: Biplane angiography and intravascular ultrasound data fusion," in *Medical Imaging 1996: Physiology and Function from Multidimensional Images*, E. A. Hoffman, ed., vol. 2709, pp. 82–92, SPIE Proceedings, (Bellingham WA), 1996.
25. M. Sonka, V. Hlavac, and R. Boyle, *Image Processing, Analysis, and Machine Vision*, PWS Publishing, Pacific Grove, 2nd ed., 1998/99.
26. W. Li, C. von Birgelen, C. Di Mario, E. Boersma, E. J. Gussenhoven, N. H. J. J. van der Putten, and N. Bom, "Semi-automatic contour detection for volumetric quantification of intravascular ultrasound," in *Proc. Computers in Cardiology 1994, Bethesda MD*, pp. 277–280, IEEE-CS Press, (Los Alamitos CA), 1994/95.
27. E. Catmull and R. Rom, "A class of local interpolating splines," in *Computer Aided Geometric Design*, R. E. Barnhill and R. F. Riesenfeld, eds., pp. 317–326, Academic Press, (New York), 1974.
28. M. Laban, J. A. Oomen, C. J. Slager, J. J. Wentzel, R. Krams, J. C. H. Schuurbiers, A. den Boer, C. von Birgelen, P. W. Serruys, and P. J. de Feyter, "ANGUS: A new approach to three-dimensional reconstruction of coronary vessels by combined use of angiography and intravascular ultrasound," in *Proc. Computers in Cardiology 1995, Vienna AT*, pp. 325–328, IEEE Press, (Piscataway NJ), 1995.
29. J. L. Evans, K. H. Ng, S. G. Wiet, M. J. Vonesh, W. B. Burns, M. G. Radvany, B. J. Kane, C. J. Davidson, S. I. Roth, B. L. Kramer, S. N. Meyers, and D. D. McPherson, "Accurate three-dimensional reconstruction of intravascular ultrasound data; spatially correct three-dimensional reconstructions," *Circulation* **93**, pp. 567–576, Feb. 1996.
30. C. Pellot, I. Bloch, A. Herment, and F. Sureda, "An attempt to 3-D reconstruct vessel morphology from X-ray projections and intravascular ultrasounds modeling and fusion," *Computerized Medical Imaging and Graphics* **20**, pp. 141–151, May/June 1996.
31. R. Shekhar, R. M. Cothren, D. G. Vince, and J. F. Cornhill, "Fusion of intravascular ultrasound and biplane angiography for three-dimensional reconstruction of coronary arteries," in *Proc. Computers in Cardiology 1996, Indianapolis IN*, pp. 5–8, IEEE Press, (Piscataway NJ), 1996.
32. W. Boehm, "Differential geometry I," in *Curves and Surfaces for Computer Aided Geometric Design: A Practical Guide*, G. E. Farin, pp. 189–199, Academic Press, (Boston), 3rd ed., 1992/93.
33. M. E. Olszewski, R. M. Long, S. C. Mitchell, A. Wahle, and M. Sonka, "Quantitative measurements in geometrically correct representation of coronary vessels in 3-D and 4-D," in *Proc. 4th IEEE Southwest Symposium on Image Analysis and Interpretation, Austin TX*, pp. 259–263, IEEE-CS Press, (Los Alamitos CA), 2000.
34. A. Wahle, S. C. Mitchell, C. von Birgelen, R. Erbel, and M. Sonka, "On-site 3-D reconstruction and visualization of intravascular ultrasound based upon fusion with biplane angiography," in *Computer Assisted Radiology and Surgery (CARS '99)*, H. U. Lemke, M. W. Vannier, K. Inamura, and A. G. Farman, eds., vol. 1191 of *Excerpta Medica International Congress Series*, pp. 56–60, Elsevier, (Amsterdam), 1999.
35. A. Wahle, S. C. Mitchell, R. M. Long, and M. Sonka, "Accurate volumetric quantification of coronary lesions by fusion between intravascular ultrasound and biplane angiography," in *Computer Assisted Radiology and Surgery (CARS 2000)*, H. U. Lemke, M. W. Vannier, K. Inamura, A. G. Farman, and K. Doi, eds., vol. 1214 of *Excerpta Medica International Congress Series*, Elsevier, (Amsterdam), 2000.